Available online at www.sciencedirect.com
ScienceDirect
Nuclear Instruments and Methods in Physics Research A 577 (2007) 275–283
NUCLEAR INSTRUMENTS & METHODS IN PHYSICS RESEARCH Section A
www.elsevier.com/locate/nima

# Theory and simulation of warm dense matter targets

J.J. Barnard[a,*], J. Armijo[b], R.M. More[b], A. Friedman[a], I. Kaganovich[c], B.G. Logan[b], M.M. Marinak[a], G.E. Penn[b], A.B. Sefkow[c], P. Santhanam[b], P. Stoltz[d], S. Veitzer[d], J.S. Wurtele[b]

[a]*L-637, Lawrence Livermore National Laboratory, Livermore, CA 94550, USA*
[b]*Lawrence Berkeley National Laboratory, Berkeley, CA 94720, USA*
[c]*Princeton Plasma Physics Laboratory, Princeton, NJ, USA*
[d]*Tech-X Corporation, Boulder, CO, USA*

Available online 22 February 2007

**Abstract**

We present simulations and analysis of the heating of warm dense matter (WDM) foils by ion beams with energy less than 1 MeV per nucleon to target temperatures of order 1 eV. Simulations were carried out using the multi-physics radiation hydrodynamics code HYDRA and comparisons are made to an analytical model and the code DPC. We simulate possible targets to be used in a proposed experiment at Lawrence Berkeley National Laboratory (the so-called Neutralized Drift Compression Experiment, NDCX II) for studies of WDM. We compare the dynamics of ideally heated targets under several assumed equations of state and explore target dynamics in the two-phase (fluid–vapor) regime.


*PACS:* 52.40.Mj; 64.60

*Keywords:* Warm dense matter; Hydrodynamics; Equation of state; Beam–plasma interactions

## 1. Introduction

The use of ion beams to heat matter to warm dense matter (WDM) conditions has been suggested due to a number of potential advantages, such as precise control and uniformity of energy deposition, large sample sizes compared to diagnostic resolution volumes, ability to heat a wide variety of target materials (both conductors and insulators), relatively long times to allow achievement of local equilibrium conditions, a benign environment for diagnostics, and high shot repetition rates. One approach (adopted at GSI, for example) has been to utilize ion beams with stopping ranges much greater in distance than the focal spot radii of the beams. Thus, these targets can be roughly cylindrical in geometry or can be planar with direction of beam incidence parallel to the face of the target. Recently, a collaboration of researchers [1] at LBNL, LLNL, and PPPL (the Heavy Ion Fusion Science Virtual National Laboratory, or HIFS VNL) has been exploring the possibility of using ions at lower energy (less than 1 MeV per nucleon) but with shorter pulse duration (~1 ns) and higher current (~100 A). The lower energy implies a very short range (~1–100 μm), which is much smaller than the radius of the focal spot (~1 mm). The geometry of such targets is thus closer to being planar with direction of beam incidence normal to the face of the target. The intent of this paper is to begin to show how equations of state, and other transport parameters of interest, will be inferred by understanding the hydrodynamics of foils as they are volumetrically heated by ion beams.

This paper is organized as follows. Section 2 outlines the basic requirements on a beam and target. Section 3 reviews the basic hydrodynamic equations and their solutions as given in Ref. [2] for idealized equations of state. Section 4 illustrates some of the complexities of the physics when the equation of state (EOS) becomes more realistic and parts of

*Corresponding author. Tel.: +1 925 423 0675; fax: +1 925 422 7390.
*E-mail address:* jjbarnard@llnl.gov (J.J. Barnard).

0168-9002/$ - see front matter © 2007 Elsevier B.V. All rights reserved.
doi:10.1016/j.nima.2007.02.062

the target enter into a two-phase (liquid–vapor) region. Section 5 describes a numerical study which parametrically explores the heating of a particular target with typical beam intensities planned for a future US experiment called NDCX II in order to determine which parameters will be most useful for inferring an unknown EOS from experimental measurements. Section 6 discusses some of the neglected physics, such as surface tension effects, which will ultimately be necessary to include in simulations in order to understand some aspects of the beam–target interaction physics.

## 2. Requirements on the beam and target

Our basic strategy [3] for carrying out WDM experiments using ion beams is to focus a low-to-moderate energy (0.4–30 MeV) (but high current) ion beam onto a thin foil target. The exact energy and ion mass are chosen such that the beam enters the foil with an energy slightly higher than the Bragg peak, and exits the foil with an energy slightly lower than the Bragg peak [4]. This allows the energy deposition to be relatively uniform through the entire depth of the target, so that precise measurements could be carried out to determine EOS, or other material properties, such as thermal and electrical conductivity, or material dielectric constant. In this paper, we focus on parameters of a proposed facility to be built at LBNL called NDCX II. One option for this facility is to use 2.8 MeV singly charged Li ions. The conclusions we draw, however, are not limited to the NDCX II facility. These high-current, low-energy beams may require compression and focusing in a neutralized plasma to overcome beam space charge, and plans and experiments for this approach are described in Refs. [1,5–11].

In order to reach WDM conditions, enough energy must be supplied to the target to raise the temperature to a regime of interest. Although a precise estimate of the target temperature requires the use of a more sophisticated EOS, to obtain an estimate, we may equate the energy density to the energy deposited divided by the volume over which the energy is deposited:

$$(M/2)nkT = \Delta E_{\mathrm{ion}}\, N_{\mathrm{ions}}/(\pi r_{\mathrm{spot}}^2\, \Delta z) \tag{1}$$

(for a uniform distribution of ion intensity at the focal plane). Here, $M$ is the number of degrees of freedom. For solids at relevant temperatures, $M = 6$ (3 kinetic plus 3 "vibrational"degrees of freedom); and $\Delta z = \Delta E_{\mathrm{ion}}/(\rho \mathrm{d}E/\mathrm{d}X)$. $\Delta E_{\mathrm{ion}}$ is the change in ion energy between entrance to and exit from the foil, chosen such that $\mathrm{d}E/\mathrm{d}X$ varies by some prescribed variance such as 5%. Typically, the entrance and exit energy ($E_{\mathrm{entrance}}$ and $E_{\mathrm{exit}}$) are chosen to be 1.5 times and 0.5 times, respectively, the energy of the peak in $\mathrm{d}E/\mathrm{d}X$. ($\mathrm{d}E/\mathrm{d}X$ and $\Delta z$ have been obtained using the SRIM code; see Figs. 1 and 2). From Fig. 1, we see that for near-term experiments which are limited to energies of a few MeV or less, only Li has the Bragg peak within the accessible range, of the three lower mass alkali metal ions that are candidates for hot plate ion sources.

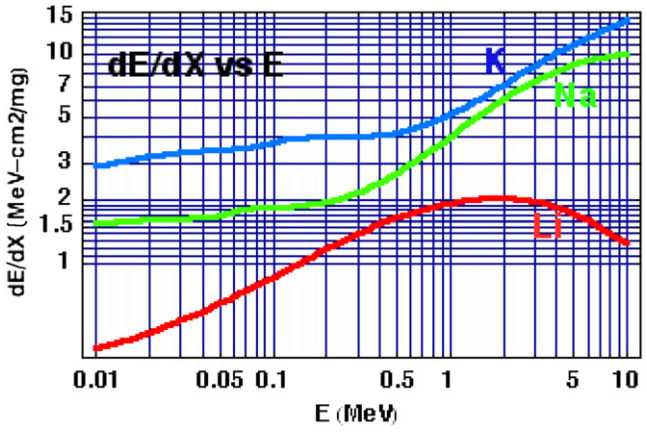


Fig. 1. Energy loss rate ($\mathrm{d}E/\mathrm{d}X$) as a function of ion energy in solid Al for three different beam ions (K, Na, and Li) for energies that include the range of current and possible near-term future experiments (data from the SRIM code).

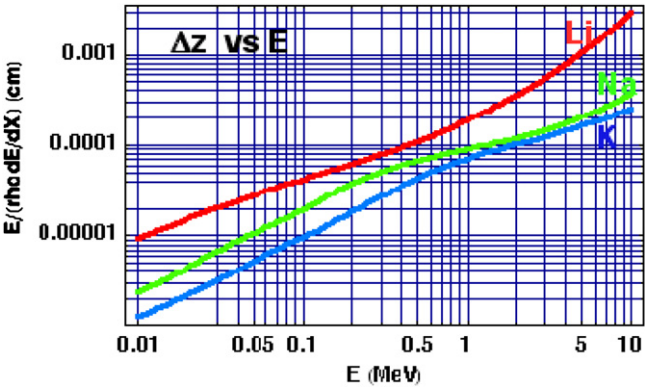


Fig. 2. Range in cm ($E/(\rho\, \mathrm{d}E/\mathrm{d}X)$ ) as a function of ion energy in solid Al for three different beam ions (K, Na, and Li) for energies that include the range of current and possible near-term future experiments (data obtained from the SRIM code).

Rearranging Eq. (1) and putting in values for Li yields:

$$kT = 9.6\,\mathrm{eV}\,(N_{\mathrm{ions}}/10^{13})\,(1\,\mathrm{mm}/r_{\mathrm{spot}})^2 \times(\mathrm{d}E/\mathrm{d}X/2\,\mathrm{MeV\,cm^2/mg})\,(A_{\mathrm{targ}}/27). \tag{2}$$

In terms of total charge $Q$:

$$kT = 6.0\,\mathrm{eV}(Q/1\,\mu\mathrm{C})\,(1\,\mathrm{mm}/r_{\mathrm{spot}})^2 \times(\mathrm{d}E/\mathrm{d}X/2\,\mathrm{MeV\,cm^2/mg})\,(A_{\mathrm{targ}}/27). \tag{3}$$

Expressed in terms of the fluence per unit area, $F$:

$$kT = 0.19\,\mathrm{eV}(F/1\,\mathrm{J/cm^2})\,(1\,\mathrm{MeV}/E_{\mathrm{entrance}}) \times(\mathrm{d}E/\mathrm{d}X/2\,\mathrm{MeV\,cm^2/mg})\,(A_{\mathrm{targ}}/27). \tag{4}$$

The fluence is defined as the energy integrated over the entire pulse. This formula uses the energy at foil entrance $E_{\mathrm{entrance}}$ and $\mathrm{d}E/\mathrm{d}X$ at foil center. For Li at the Bragg Peak, $E_{\mathrm{peak}} = 1.88$ MeV, $\mathrm{d}E/\mathrm{d}X = 2.052\,\mathrm{MeV\,cm^2/mg}$. The entrance to the foil is approximately at 50% high energy,

$E_{\text{entrance}} = 2.82\,\text{MeV}$. Thus, to reach 2 eV (to allow for some robustness for the experiments) requires: $F = 29.1$ J/cm$^2$ o f Li at $E_{\text{entrance}} = 2.82\,\text{MeV}$.

Using Eqs. (1)–(4), similar estimates can be made for other experiments using K and Na.

The basic beam requirement is thus the fluence per unit area $F$, which must be delivered to raise the target temperature to values of interest. However, a second important parameter is the pulse duration, $\Delta t$. The pulse duration must be sufficiently short relative to the cooling timescale, which for this regime is typically the hydrodynamic timescale $t_{\text{hydro}} = \Delta z/c_s$, such that significant cooling has not occurred. Here, $c_s$ is the sound speed (at the temperature of the heated material.) For Al at 1 eV the sound speed is approximately $5 \times 10^5$ cm/s so that for a 3.5 μm foil, the hydrodynamic timescale is about 0.7 ns. Pulse durations significantly longer than 1 ns would thus not reach the desired temperature. Fig. 2 shows the benefit of using Li for low energy experiments, since the larger range at solid density leads to longer hydrodynamic timescales. Thus, for experiments at solid densities, hydro simulation codes are required to ensure that central temperatures of interest can be achieved, when beam pulse durations $\Delta t$ are roughly the same order as $t_{\text{hydro}}$.

### 2.1. Foam targets

Targets made of metallic foams are of interest in their own right, because of their use in Inertial Confinement Fusion and other applications, but also as a means of relaxing the pulse duration requirements on the beam for the purpose of exploring a wide range of parameters in the density–temperature parameter space. For metallic foam with a mass density equal to 10% of solid density, the ion range $\Delta z$ increases by a factor of 10 over its value for solid density, and so the hydrodynamic timescale increases by that factor also. With foams, it is much easier to be in a regime where the pulse duration $\Delta t \ll t_{\text{hydro}}$. The main issue with foams is that they are inherently inhomogeneous. The timescale for homogenization is approximated as $t_{\text{uniform}} \backsim nr/c_s$ where $n$ is a number of order 3–5, $r$ the pore size and $c_s$ the sound speed. Thus, for $n = 4$, $r = 100$ nm, the homogenization time would be 1% of the hydro timescale for a 40 μm, 10% Al foam foil. Foams with 100 nm pore size should be obtainable, according to LLNL ICF researchers. This factor of 100 in the separation of timescales should be sufficient for our purposes of obtaining EOS data in the WDM regime. However, we should also note that the critical point is typically near one-third solid density and the liquid-two-phase transition boundary at lower temperatures is at even higher densities, so the ability to operate up to solid density is important for the robustness of any WDM facility.

We should also note that ion stopping may be affected when the time between collisions is longer than the relaxation timescale of the ion in the excited state. Measurements of ion stopping in foam could provide information regarding the fundamental science of ion stopping.

## 3. Analytic theory using ideal gas EOS

The continuity equation for the mass density $\rho$, fluid velocity $v$, evolving in time $t$ and longitudinal coordinate $z$ may be written:

$$\frac{\partial \rho}{\partial t} + \frac{\partial \rho v}{\partial z} = 0. \tag{5}$$

The momentum equation can be written:

$$\frac{\partial v}{\partial t} + v\,\frac{\partial v}{\partial z} = -\frac{1}{\rho}\,\frac{\partial p}{\partial z}. \tag{6}$$

For an adiabatic change in the material the pressure satisfies

$$p = K\rho^{\gamma}. \tag{7}$$

Here $K$ is a constant ($= p_0/\rho_0^{\gamma}$, where subscript 0 indicates initial values). The sound speed in the medium is give by: $c_s^2 \equiv \gamma P/\rho\cdot$ A similarity solution is found in the variable $z/c_{s0}t$ for the evolution of a rarefaction wave which initially propagates into an uniform medium (for $z>0$) with pressure $p_0$, density $\rho_0$, and sound speed $c_{s0}$, and subsequently expands into what is initially a vacuum for $z<0$. The solution (the so-called simple wave solution) in the region $-2/(\gamma-1) < z/c_{s0}t < 1$ is given by [2]

$$\frac{v}{c_{s0}} = \left(\frac{2}{\gamma+1}\right)\left(\frac{z}{c_{s0}t} - 1\right) \tag{8}$$

$$\frac{c_s}{c_{s0}} = \left(\frac{\gamma-1}{\gamma+1}\right)\left(\frac{z}{c_{s0}t}\right) + \frac{2}{\gamma+1} \tag{9}$$

$$\frac{\rho}{\rho_0} = \left(\frac{c_s}{c_{s0}}\right)^{2/(\gamma-1)}; \quad \frac{T}{T_0} = \left(\frac{c_s}{c_{s0}}\right)^2. \tag{10}$$

Consider a slab of finite width $2L$. In that case, a rarefaction wave will propagate into the medium at speed $c_{s0}$ from both edges of the slab ($z = 0$ and $z = 2L$). Let $\tau = c_{s0}t/L$ and $\zeta = z/L$. After $\tau = 1$, the simple waves will collide and there will be a growing region (the non-simple wave region) not governed by Eqs. (8)–(10).

The boundary between the simple waves and the non-simple waves is given [2] by

$$\zeta_{\text{boundary}} = \frac{-2}{(\gamma-1)}\tau + \left(\frac{\gamma+1}{\gamma-1}\right)\tau^{(3-\gamma)/(\gamma+1)}. \tag{11}$$

In Ref. [2], it is shown how Eqs. (5)–(7) may be transformed into a single, second order partial differential equation for the transformed variable $\chi$, expressed as a function of the velocity $v$ and the enthalpy $w = c_s^2/(\gamma-1)$:

$$\frac{2}{2n+1}\,w\,\frac{\partial^2 \chi}{\partial w^2} - \frac{\partial^2 \chi}{\partial v^2} + \frac{\partial \chi}{\partial w} = 0. \tag{12}$$

What are normally the independent variables $z$ and $t$ may be generated from

$$t = \partial\chi/\partial w; \quad z = v\partial\chi/\partial w - \partial\chi/\partial v. \tag{13}$$

The general solution is [2]

$$\chi = \left(\frac{\partial}{c_s\partial c_s}\right)^{n-1}\left(\frac{1}{c_s}F_1\left(c_s + \frac{v}{2n+1}\right) + \frac{1}{c_s}F_2\left(c_s - \frac{v}{2n+1}\right)\right). \tag{14}$$

Here $F_1$ and $F_2$ are arbitrary functions, and the solution is valid for positive integral values of $n$, where $n = (3-\gamma)/(2(\gamma-1))$.

The particular solution with $v = 0$ at $z/L = 1$, and $\chi = 0$ along a boundary curve is [2]

$$\chi = \frac{L(2n+1)}{2^n n!}\left(\frac{\partial}{c_s\partial c_s}\right)^{n-1}\left(\frac{1}{c_s}\left[\left(c_s - \frac{v}{2n+1}\right)^2 + c_{s0}^2\right]^n\right). \tag{15}$$

So, for a given value of $n$, one may calculate $\chi$, then take its derivatives with respect to $c_s$ and $v$ in order to find $t(c_s,v)$ and $z(c_s,v)$, and finally invert the solution, if possible. For example, for $\gamma = 5/3$, ($n = 1$, corresponding to a perfect gas with 3 degrees of freedom), the solution becomes: $\chi = L(9c_s^2 - 9c_{s0}^2 - 6c_s v + v^2)/(6c_s)$; $t = L(9c_s^2 + 9c_{s0}^2 - v^2)/(18c_s^3)$; and $z = L(18c_s^3 + 3c_s^2 v + 9c_{s0}^2 v - v^3)/(18c_s^3)$.

From observation of the exact solution, we find the velocity in the non-simple region is nearly linear starting from zero at the center of the slab ($\zeta = 1$) to the value $v = v(\zeta = \zeta_{\text{boundary}})$ on the boundary between the simple and non-simple wave. So, an approximate solution $v_{\text{approx}}/c_{s0}$ for the velocity in this region ($\zeta_{\text{boundary}} < \zeta < 1$, and $\tau > 1$) is given by

$$\frac{v_{\text{approx}}}{c_{s_0}} = \frac{-2}{\gamma-1}(1 - \tau^{2(1-\gamma)/(\gamma+1)})\left(\frac{\zeta-1}{\zeta_{\text{boundary}}-1}\right). \tag{16}$$

Similarly, the density in the non-simple wave region is observed to be nearly parabolic from center to the edge. Using conservation of total mass, and using the value of $\rho/\rho_0$ on the boundary $\zeta = \zeta_{\text{boundary}}$, it is easy to calculate the approximate density in the non-simple region ($\zeta_{\text{boundary}} < \zeta < 1$):

$$r_{\text{approx}} \equiv \frac{\rho}{\rho_0} = (r_{\max} - \tau^{-4/(\gamma+1)}) \times\left(1 - \left(\frac{\zeta-1}{\zeta_{\text{boundary}}-1}\right)^2\right) + \tau^{-4/(\gamma+1)} \tag{17}$$

where $r_{\max}$ is the value of $\rho/\rho_0$ at the center of slab ($\zeta = 1$) and is given by

$$r_{\max} = \frac{3(1 - \tau^{-1} - \frac{1}{3}\tau^{-4/(\gamma+1)}(1 - \zeta_{\text{boundary}}))}{2(1 - \zeta_{\text{boundary}})}. \tag{18}$$

Thus, the simple wave solution (Eqs. (8)–(10)), together with either the exact formula (Eq. (15)) or the approximate formulas in the non-simple wave region (Eqs. (16)–(18)), give the complete solution to the evolution of a one-dimensional slab which is heated instantaneously to some temperature $T_0$, assuming a perfect gas EOS. (The solutions are for $\zeta < 1$; the $\zeta > 1$ solution is obviously a mirror image of the $\zeta < 1$ solution). The approximate formulas are more tractable and can be useful for understanding the scaling of the central part of the slab (for example), and for non-integer values of $n$. This ideal solution for a perfect gas can be used as a reduced model or starting point for interpretation of more complicated situations in which there is a non-ideal EOS, or when beam energy deposition occurs over a finite time, or when the deposition is not entirely uniform. The main features of the solution are the expansion of the material outward at a velocity $v = \pm 2c_{s0}/(\gamma-1)$, a rarefaction wave propagating inward at velocity $c_{s0}$, and a decreasing central density (and temperature) for times after the rarefaction wave has reached the center of the slab ($\tau = 1$).

## 4. Simulation results under instantaneous heating approximation

A more sophisticated treatment of the cases treated by the analytical model outlined in Section 3 requires the use of numerical simulation codes. Two codes have been employed in this study. The code HYDRA [12] is a 3D radiation/hydrodynamics code used primarily for ICF simulations, and has been employed here for target hydrodynamics. The 1D hydrodynamics code DPC (written by Richard More), uses an EOS specifically formulated for the WDM regime, based on the Saha equation using energy levels of neutral atoms, melting temperature and latent heat of the material studied [13]. DPC has also been extensively employed for hydrodynamics calculations of the target. Since the beam radius is of order 1 mm, and the thickness of the target is of order a few μm for a solid, to a few hundred μms for a 1% foam, the 1D code should accurately represent the longitudinal physics at the center of the target. DPC uses a Maxwell construction for the EOS [13]. In the Maxwell construction, an isotherm of the EOS that has a region in $\rho$ that is dynamically unstable in the two-phase regime ($\partial P/\partial\rho < 0$) is replaced by an isotherm with a region of constant pressure as a function of density that bridges the transition in density between pure liquid and pure vapor. This construction yields the equilibrium value of pressure, and yields numerically stabler solutions, but does not resolve the material into bubbles and droplets. HYDRA has been employed using two different equations of state, QEOS [14] and LEOS, the latter of which employs a tabular EOS. QEOS uses a Thomas Fermi model for the electron EOS and uses a modified Cowan model for the ion EOS. QEOS does not use the Maxwell construction, but LEOS allows use of either the Maxwellian or non-Maxwellian construction.

Recently, in Ref. [15], DPC was used to study the expansion of a tin (Sn) foil which is initially in a liquid state, but due to expansion of the foil, transitions into the two-phase regime, where liquids and vapors coexist.

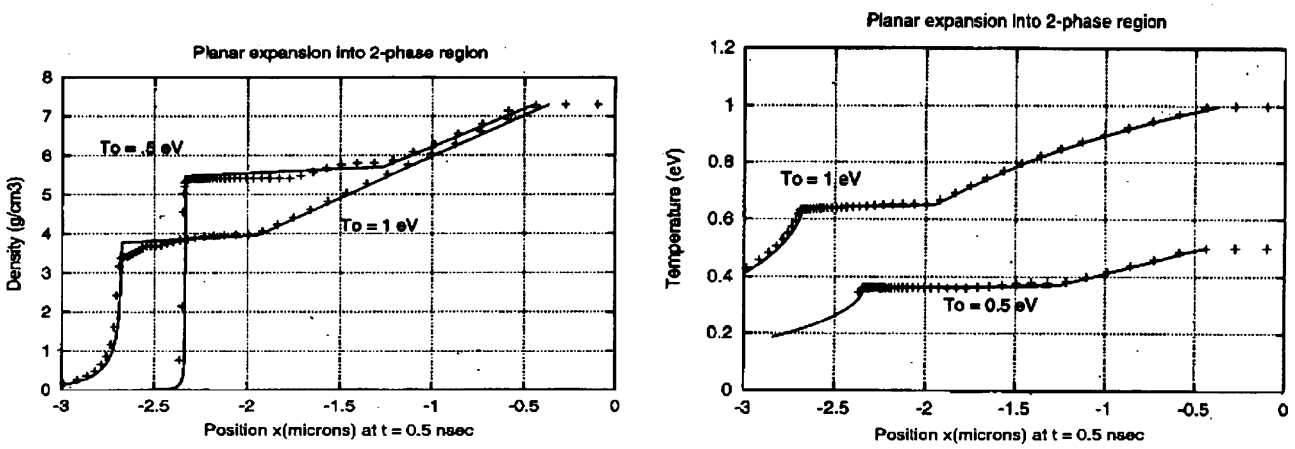


Fig. 3. Snapshot of tin (symbol) foil, with initial temperature $T_0$ of 0.5 and 1.0 eV after 0.5 ns. The surface of the foil was initially at $-2\,\mu$m in this DPC simulation (left: density vs. position; right: temperature vs. position) (from Ref. [15]).

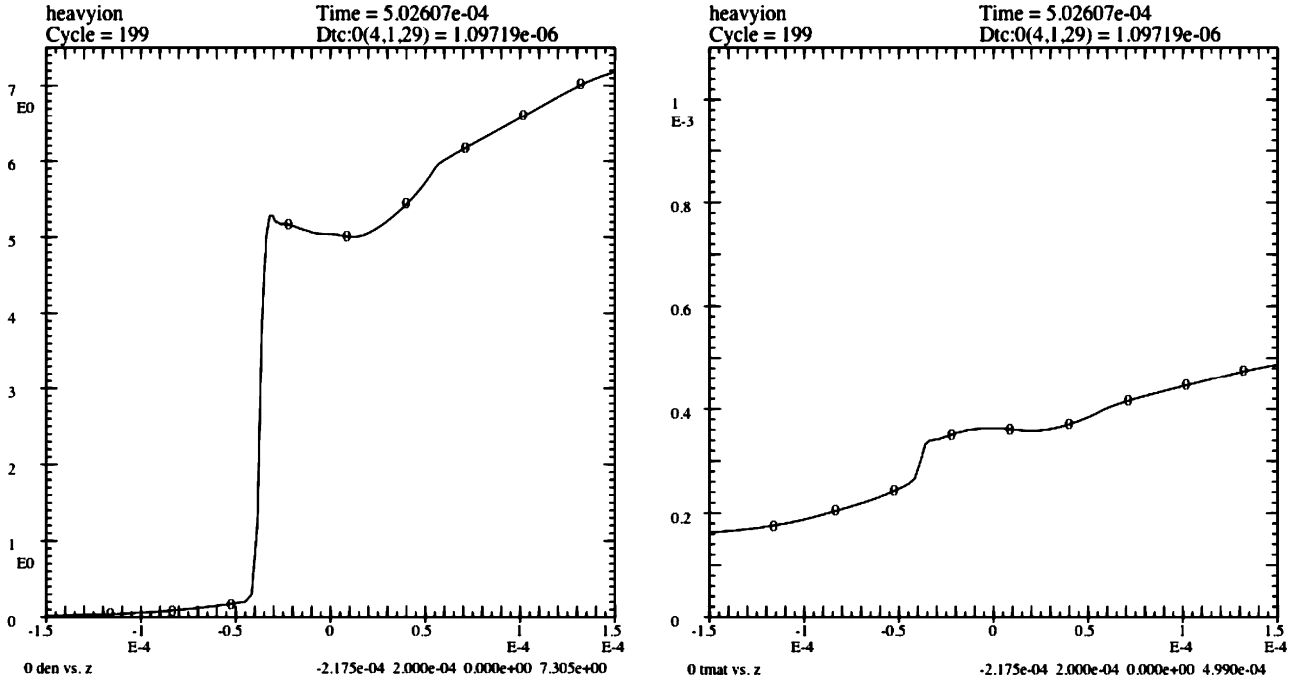


Fig. 4. Snapshot of tin (Sn) foil, with initial temperature $T_0$ of 0.5 eV after 0.5 ns. The surface of the foil was initially at 0 μm in this HYDRA/QEOS simulation (left: density (g/cm$^3$) vs. position (cm) (Here 1E-4 corresponds to $1 \times 10^{-4}$ cm = 1 micron); right: temperature (keV, [here 1E-3 keV corresponds to 1 eV]) vs. position (cm)).

Fig. 3 shows the results. Plateaus in densities and temperatures are apparent in the spatial profiles as time elapses and the material undergoes a phase transition. When HYDRA is run using QEOS and without the Maxwell construction, evidence for the plateaus remains at roughly the same longitudinal position (see Figs. 4 and 5), although oscillations in density are apparent as the code tries to make bubbles (vapor density) and droplets (liquid density) in the two-phase region. The spatial zoning is likely not fully resolving the droplets and bubble formation and the code does not include surface tension effects, so the limits and assumptions of the simulation should be kept in mind.

## 5. Parametric studies for NDCX II

To understand the general physics of the beam–target interaction in the context of a particular experiment, we have chosen a set of ion beam and target parameters similar to those proposed for the NDCX II experiment, which is proposed by the HIFS VNL [1]. In particular, we have modeled the dynamics of solid Al targets that have been heated by a 2.8 MeV $Li^+$ ion beam, one possible ion species and energy option for NDCX II. (2.8 MeV corresponds to an energy 50% higher than the Bragg peak energy, resulting in an approximately 5% variation in $dE/dX$, if a foil thickness is chosen such that the beam exits

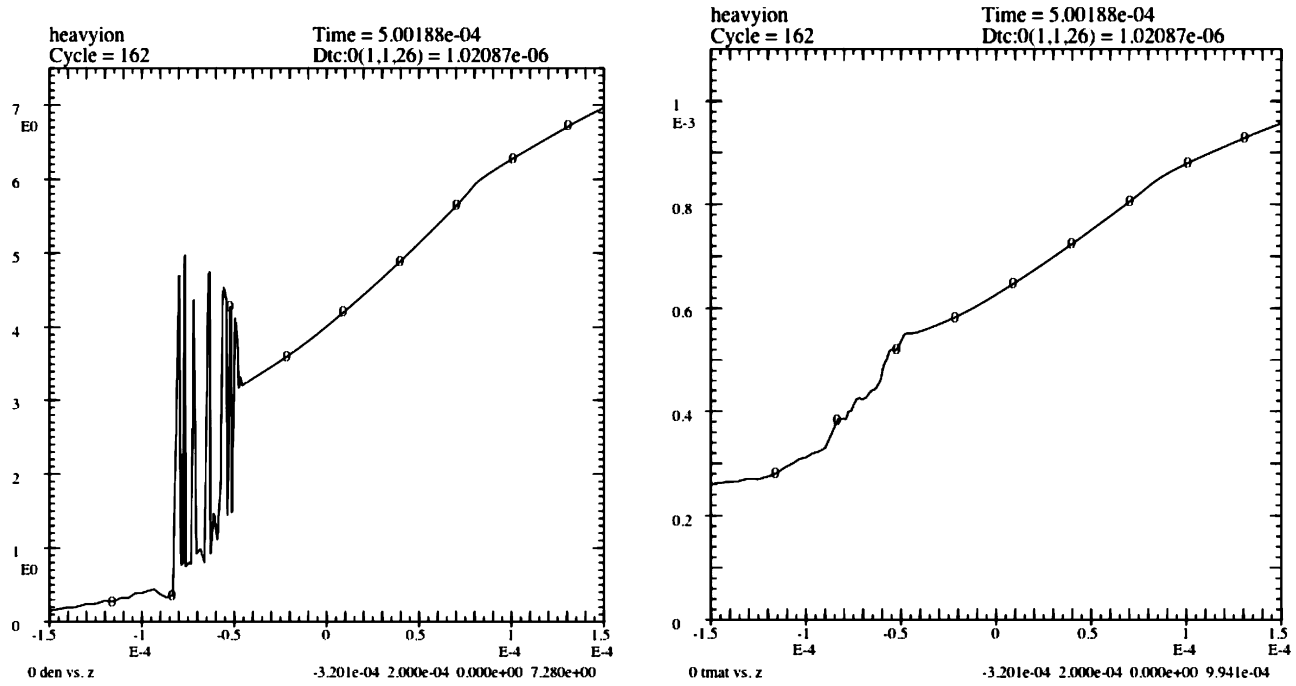


Fig. 5. Snapshot of tin (symbol) foil, with initial temperature $T_0$ of 1.0 eV after 0.5 ns. The surface of the foil was initially at 0 microns in this HYDRA/QEOS simulation (left: density (g/cm$^3$) vs. position (cm) (Here 1E-4 corresponds to $1 \times 10^{-4}$ cm = 1 micron); right: temperature (keV, [here 1E-3 keV corresponds to 1 eV]) vs. position (cm)).

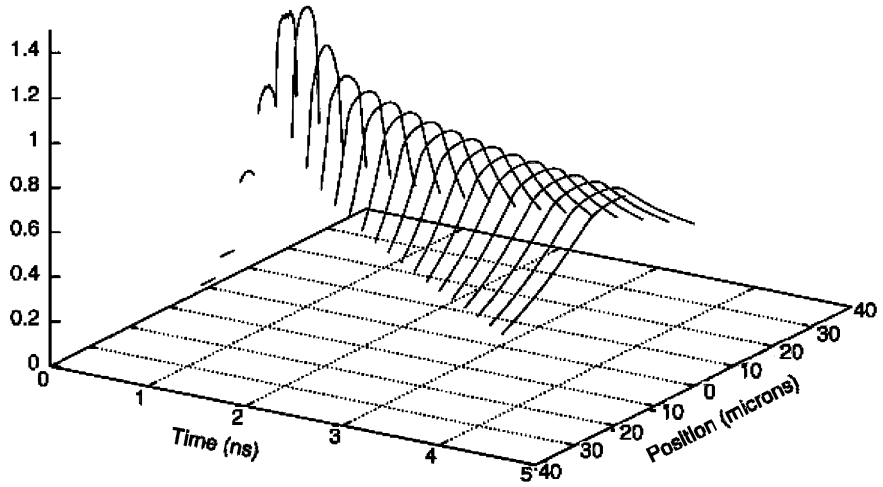


Fig. 6. Target temperature as a function of time and position for the nominal Li NDCX II parameters using the DPC code over the first 5 ns. The foil is initially 3.5 μm thick (centered at $z = 0$) and has expanded to cover 20–30 μm after approximately 4 ns.

the foil at approximately 0.93 MeV, or half the energy at the Bragg peak). Other parameters for the "nominal" case include an ion fluence per unit area $F$ impinging on the target of 30 J/cm$^2$ and an initial d$E$/d$X$ of 2.052 MeV-cm$^2$/mg (as estimated by the SRIM code). The energy absorbed per mass $= F$ d$E$/d$X$/ $E = 21.986$ J/mg $= 2.2 \times 10^4$ J/g $=$ 6.2 eV/atom. Thus, the nominal target temperature, assuming a specific heat of 3 eV/(eV-atom), would be approximately 2 eV. The assumed pulse duration is 1 ns, full-width in a parabolic pulse. The nominal target was solid Al ($A = 26.98$, density $= 2.7$ g/cm$^3$) with a nominal thickness of 3.5 μm. The pulse duration, target thickness and cumulative beam fluence were varied, and runs were made in the two simulation codes described above, DPC and HYDRA.

Figs. 6 and 7 show the temporal and spatial results of the nominal case from DPC. Fig. 8 shows a comparison between DPC results and results of HYDRA using QEOS, of the evolution of the central temperature of the target. Detailed differences arising from different assumptions about the EOS are apparent. Finally, some of the systematic variations in maximum central pressure, maximum central temperature and maximum surface

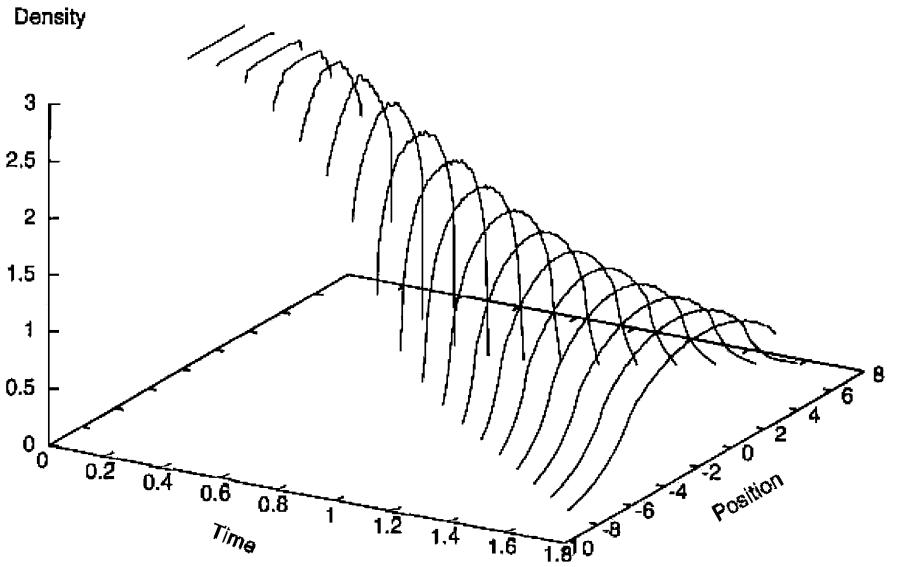


Fig. 7. Evolution of the target density as a function of time and position for the nominal Li NDCX II parameters using the DPC code (for the first 1.8 ns).

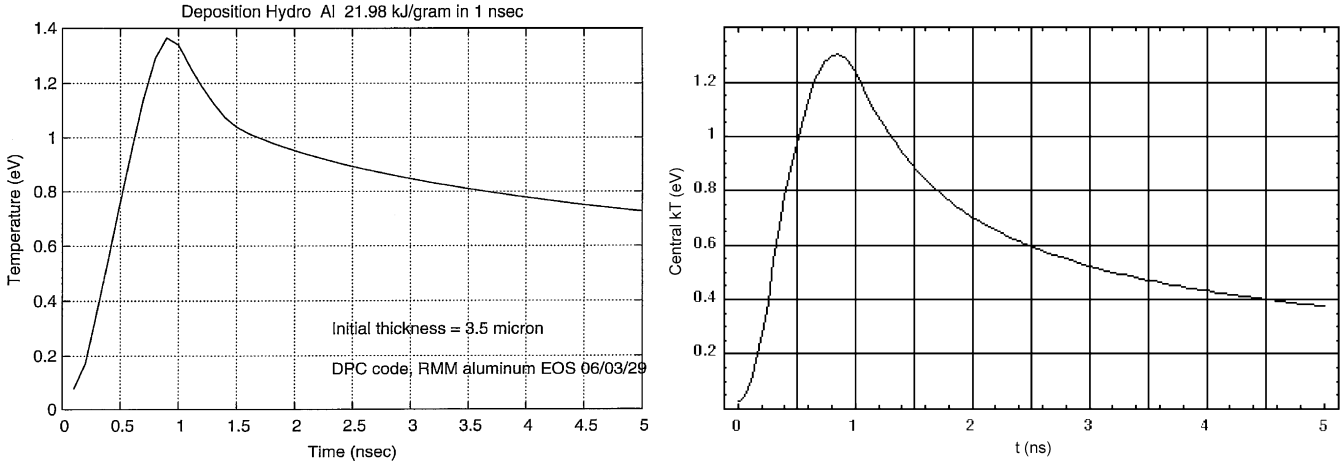


Fig. 8. Comparison of the evolution of the central temperature of the nominal case using DPC (left) and Hydra (right). The change in slope at about 1.5 ns in the DPC result has been found to be associated with the entrance into the two-phase regime.

velocity with deposition energy per target mass ($F\mathrm{d}E/\mathrm{d}X/E$) are shown in Figs. 9–11 for various target thicknesses.

Some observations from these figures can be made. The maximum central pressure achieved depends sensitively on the foil thickness (as well as the energy deposition), since different thicknesses allow the rarefaction wave to reach the center of the foil before all of the energy from the ion beam has been deposited. The pressure is most sensitive to target thickness because it depends on both density and temperature decreases. The temperature also is reduced for thinner foils because of the cooling during expansion, but the ion deposition continues to increase the central temperature after the rarefaction wave has reached the center. The expansion velocity is the least sensitive to the foil thickness, perhaps because it reflects an integrated effect of the energy deposited [19]. We should note that for the solution of the instantaneously heated perfect gas foil described in Section 3, we may write the energy density per mass $\varepsilon = c_{s0}^2/(\gamma(\gamma-1))$, so that the maximum expansion velocity of the outward material can be expressed $v = (4\gamma/(\gamma-1)^{1/2}\varepsilon^{1/2}$. So, for this case, the ratio of the velocity to the energy deposition depends only on the EOS (i.e. $\gamma$ in this model), which suggests that measurements of expansion velocity will be useful in determining unknown equations of state in planned near-term experiments.

## 6. Capturing the physics of bubbles and droplets

As discussed above, neither DPC nor HYDRA captures the detailed physics of droplets or bubbles, which may be important in understanding the results of WDM experiments using ion beams. One deficiency is the lack of surface tension effects in either code.

We have begun to estimate the maximum size of droplets that would be created in the transition of the expanding foil from liquid to gas. In one estimate, the force on a droplet

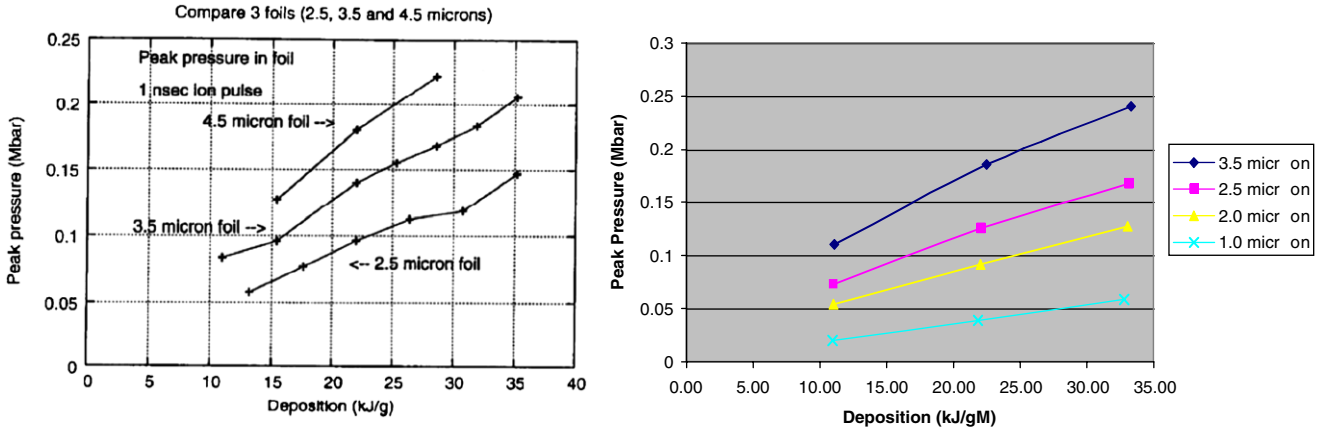


Fig. 9. Peak pressure vs. energy deposition for three foil thicknesses (see text for parameters) using the DPC code (left) and four foil thicknesses (3.5 [uppermost], 2.5, 2.0, and 1.5 microns [lowermost]) using HYDRA/QEOS.

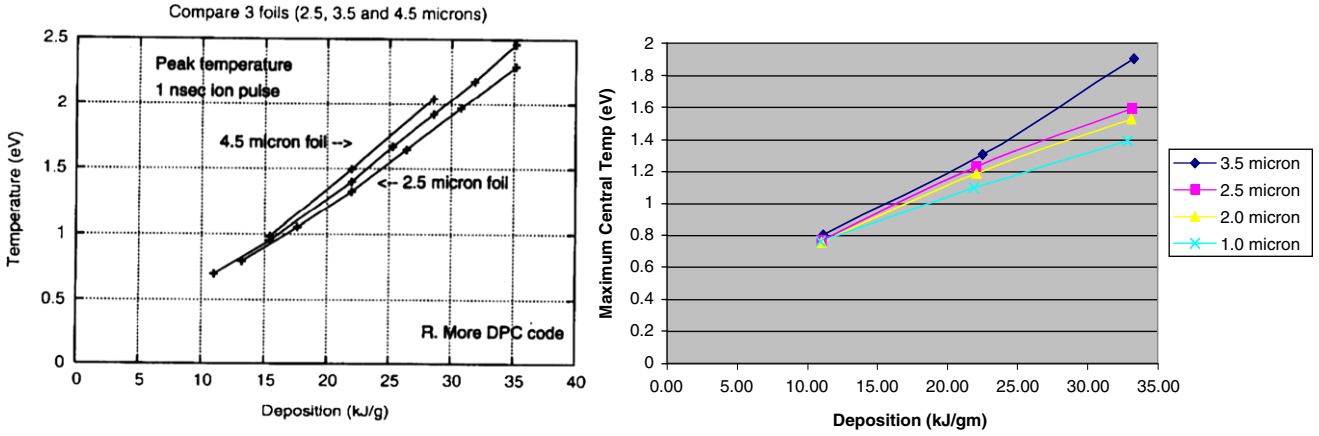


Fig. 10. Peak temperature vs. energy deposition for three foil thicknesses (see text for parameters) using the DPC code (left) and four foil thicknesses (3.5 [uppermost], 2.5, 2.0, and 1.5 microns [lowermost]) using HYDRA/QEOS.

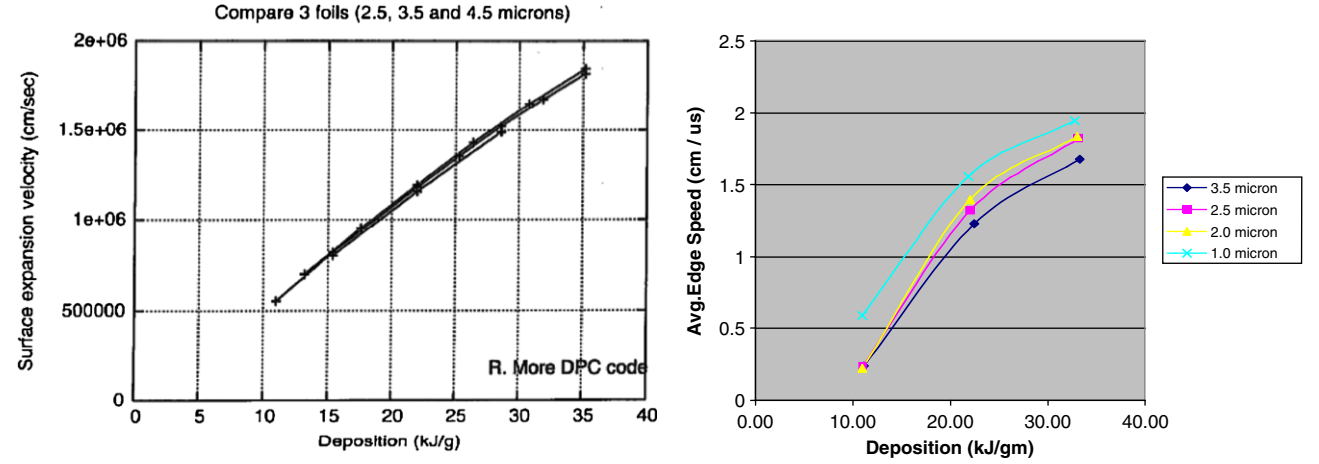


Fig. 11. Release velocity vs. energy deposition vs. for three foil thicknesses (see text for parameters) using the DPC code (left) and four foil thicknesses (3.5 [lowermost], 2.5, 2.0, and 1.5 microns [uppermost]) using HYDRA/QEOS.

from the viscosity of the expanding gas tending to stretch the droplet will overcome the inward force of the surface tension if the radius of the droplet is sufficiently large. This yields a maximum droplet radius $x$ given by [16]

$$x = \sigma/(\mu\, \mathrm{d}v/\mathrm{d}x). \tag{19}$$

This corresponds to a capillary number ($\equiv \mu v/\sigma$) of order unity at the maximum radius. Here, $\sigma$ is the coefficient of surface tension, $\mu$ is the viscosity and $dv/dx$ the velocity gradient of the underlying expanding medium. Another estimate balances the dynamic pressure of an expanding droplet to the inward force of the surface tension. This yields a maximum droplet radius given by

$$x = (\sigma/\rho(dv/dx)^2)^{1/3}. \quad (20)$$

Here, $\rho$ is the liquid droplet density. This corresponds to a Weber number ($\equiv \rho x v^2/\sigma$) of order unity at the maximum radius. For typical numbers at a time when the material is in the two-phase regime ($dv/dx = 10^6$ cm/s, $\sigma = 100$ dyn/cm, $\mu = 5 \times 10^{-3}$ g/cm s, $\rho = 1$ g/cm$^3$, $v_{th} = 5 \times 10^5$ cm/s), Eq. (19) yields a maximum droplet radius of 0.20 μm, and Eq. (20) yields a maximum droplet radius of 0.05 μm, both of order 0.1 μm. (The difference between the two estimates is likely smaller than the uncertainties in the calculations, since geometrical factors were generally set to unity). Further calculations, including evaporation and condensation rates and accurate estimates of $\sigma$ and $\mu$, are beginning to yield insight into the physics of the droplets and bubbles, which may be useful as these effects are incorporated into the simulation codes.

## 7. Summary

We have analyzed, using a reduced model and a variety of simulations, the hydrodynamics of target expansion in order to provide insight into planned future experiments using ion beams to heat material to WDM conditions. Many issues still remain to be studied in more detail. In particular, foam homogenization, hydrodynamics through the two-phase region, effects of velocity spread and straggling [18] of the ion beam, and acceptable levels of preheat [17] are some of the issues which need to be evaluated. The ultimate goal of these simulation studies is to determine which observables will be most sensitive and allow minimization of uncertainties in equations of state, and other material quantities, for a wide range of target choice and over a large range in density and temperature parameter space.

## References


[1] B.G. Logan, et al., Recent US advances in ion-beam-driven high energy density physics and heavy ion fusion, Nucl. Instr. and Meth. A (2007), doi:10.1016/j.nima.2007.02.070.

[2] L.D. Landau, E.M. Lifshitz, Fluid Mechanics, Pergamon Press, New York, 1959 (Chapter 10).

[3] B.G. Logan, R.C. Davidson, J.J. Barnard, R. Lee, A unique US approach for accelerator driven warm dense matter research—preliminary report, in: Proceedings of the Workshop on Accelerator-Driven High Energy Density Physics, Appendix A1, held at LBNL, October 26–29, 2004, LBNL-57518, UCRL-PROC-212000, 2005 〈http://hifweb.lbl.gov/public/hedpworkshop/toc.html〉.

[4] L.R. Grisham, Moderate energy ions for high energy density physics experiments, Phys Plasmas 11 (2004) 5727.

[5] F.M. Bieniosek, J. Barnard, M.A. Leitner, A.W. Molvik, R. More, P.K. Roy, Diagnostics for near term WDM experiments, Nucl. Instr. and Meth. A (2007), doi:10.1016/j.nima.2007.02.063.

[6] P.K. Roy, S.S. Yu, S. Eylon, E. Henestroza, A. Anders, E.P. Gilson, F.M. Bieniosek, W.G. Greenway, B.G. Logan, W.L. Waldron, D.B. Shuman, D.L. Vanecek, D.R. Welch, D.V. Rose, C. Thoma, R.C. Davidson, P.C. Efthimion, I. Kaganovich, A.B. Sefkow, W.M. Sharp, Nucl. Instr. and Meth. A 544 (2005) 225.

[7] J.J. Barnard, R.J. Briggs, D.A. Callahan, R.C. Davidson, A. Friedman, L. Grisham, E.P. Lee, R.W. Lee, B.G. Logan, C.L. Olson, D.V. Rose, P. Santhanam, A.M. Sessler, J.W. Staples, M. Tabak, D.R. Welch, J.S. Wurtele, S.S. Yu, Accelerator and ion beam tradeoffs for studies of warm dense matter, in: Proceedings of the Particle Accelerator Conference, May 2005, Knoxville, TN, RPA039, 2005.

[8] P.K. Roy, S.S. Yu, E. Henestroza, A. Anders, F.M. Bieniosek, J. Coleman, S. Eylon, W.G. Greenway, M. Leitner, B.G. Logan, W.L. Waldron, D.R. Welch, C. Thoma, A.B. Sefkow, E.P. Gilson, P.C. Efthimion, Davidson, Phys. Rev. Lett. 95 (2005) 234801.

[9] P.K. Roy, S.S. Yu, E. Henestroza, A. Anders, D. Baca, F.M. Bieniosek, J. Coleman, R.C. Davidson, P.C. Efthimion, S. Eylon, E.P. Gilson, W.G. Greenway, I. Kaganovich, M. Leitner, B.G. Logan, A.B. Sefkow, P. Seidl, Nucl. Instr. and Meth. A (2007), doi:10.1016/j.nima.2007.02.056.

[10] A. Sefkow, R.C. Davidson, I.D. Kaganovich, E.P. Gilson, P.K. Roy, S.S. Yu, P.A. Seidl, D.R. Welch, D.V. Rose, J.J. Barnard, Optimized simultaneous transverse and longitudinal focusing of intense ion beam pulses for warm dense matter applications, Nucl. Instr. and Meth. A (2007), doi:10.1016/j.nima.2007.02.064.

[11] D.R. Welch, D.V. Rose, C. Thoma, A.B. Sefkow, I.D. Kaganovich, P.A. Seidl, S.S. Yu, J.J. Barnard, P.K. Roy, Nucl. Instr. and Meth. A (2007), doi:10.1016/j.nima.2007.02.057.

[12] M.M. Marinak, G.D. Kerbel, N.A. Gentile, O. Jones, D. Munro, S. Pollaine, T.R. Dittrich, S.W. Haan, Phys. Plasmas 8 (2001) 2275.

[13] R. More, H. Yoneda, H. Morikami, JQSRT 99 (2006) 409.

[14] R. More, K.H. Warren, D.A. Young, G.B. Zimmerman, A new quotidian equation of state for hot dense matter, Phys. Fluids 31 (1988) 3062.

[15] R. More, T. Kato, H. Yoneda, Unpublished report, National Institute for Fusion Science, Toki, Japan, 2005.

[16] J. Armijo, Master's internship report, Ecole Normale Superieure, Paris, 2006 (also LBNL-61975, Lawrence Berkeley National Laboratory).

[17] D.R. Welch, D.V. Rose, A.B. Sefkow, Avoiding preheat in a Warm Dense Matter Experiment, Workshop on Accelerator Driven Warm Dense Matter Physics, Pleasanton, CA, February 2006 〈http://hifweb.lbl.gov/public/AcceleratorWDM/TableOfContents.html〉.

[18] S. Vetzer, P.H. Stoltz, J.J. Barnard, Evolution of energy distribution of ions moving in Aluminum targets, Nucl. Inst. and Meth. A (2007), doi:10.1016/j.nima.2007.02.089.

[19] G. Guethlein, Hydrodynamics experiments on ETAII, in: Workshop on Accelerator Driven Warm Dense Matter Physics, Pleasanton, CA, February 2006 〈http://hifweb.lbl.gov/public/AcceleratorWDM/TableOfContents.html〉.